Salt-Dependent Rheology and Surface Tension of Protein Condensates Using Optical Traps

Louise M. Jawerth,[1,2,3] Mahdiye Ijavi,[1] Martine Ruer,[1] Shambaditya Saha,[1] Marcus Jahnel,[1,4]
Anthony A. Hyman,[1,3] Frank Jülicher,[2,3,*] and Elisabeth Fischer-Friedrich[1,2,4,†]

[1]*Max-Planck-Institut für Zellbiologie und Genetik, Pfotenhauerstraße 108, 01307 Dresden, Germany*
[2]*Max-Planck-Institut für Physik komplexer Systeme, Nöthnitzerstraße 38, 01187 Dresden, Germany*
[3]*Center for Systems Biology Dresden, Pfotenhauerstraße 108, 01307 Dresden, Germany*
[4]*Biotechnology Center, Technische Universität Dresden, Tatzberg 47-49, 01307 Dresden, Germany*

An increasing number of proteins with intrinsically disordered domains have been shown to phase separate in buffer to form liquidlike phases. These protein condensates serve as simple models for the investigation of the more complex membraneless organelles in cells. To understand the function of such proteins in cells, the material properties of the condensates they form are important. However, these material properties are not well understood. Here, we develop a novel method based on optical traps to study the frequency-dependent rheology and the surface tension of P-granule protein PGL-3 condensates as a function of salt concentration. We find that PGL-3 droplets are predominantly viscous but also exhibit elastic properties. As the salt concentration is reduced, their elastic modulus, viscosity, and surface tension increase. Our findings show that salt concentration has a strong influence on the rheology and dynamics of protein condensates suggesting an important role of electrostatic interactions for their material properties.

Introduction.—A fundamental question of biology is to understand the spatial organization of cells into compartments of distinct chemical composition and activity. Many cellular compartments are bounded by membranes. However, cells also possess compartments that are not bounded by membranes. Examples are germline granules, cajal bodies, nucleoli, and stress granules. It has been shown in recent years that many membraneless compartments are protein condensates forming soft materials that coexist with the cytoplasm or nucleoplasm and often exhibit liquidlike properties [1–10].

Liquidlike compartments typically contain one or two scaffold proteins which are required for compartment formation and to which RNA and other proteins colocalize [1,4,11]. Many scaffold proteins phase separate *in vitro* when introduced into physiological buffer resulting in the condensation of liquidlike droplets. A well-studied example of a phase-separating scaffold protein is PGL-3—a major component of P granules, the germline granules of the nematode worm *Caenorhabditis elegans* [2,6,11,12]. This and other protein droplets serve as models for the soft materials that form the more complex liquidlike compartments in cells [5–7,10,12,13]. The material properties of protein droplets are important to understand the biological function of protein condensates in cells—for example, when they serve as biochemical reaction centers, which requires rapid diffusion of components, or when they serve as structural elements, which may require some degree of elasticity. However, the material properties and rheology

have not yet been fully characterized. Active microrheological methods that could provide such information for micron-sized droplets are currently lacking.

The saturation concentration of protein phase separation *in vitro* depends on buffer conditions such as salt concentration, *p*H, or the presence of RNA [6,7,10,12–14]. The salt and *p*H dependence of the saturation concentration suggests a role of charge and electrostatic interactions in protein phase separation.

In this Letter, we develop a novel active microrheology method to determine the frequency-dependent rheology of micron-sized PGL-3 droplets as a function of salt concentration using optical traps. Protein droplets are deformed via two opposing adhered beads trapped by optical traps [Figs. 1(a), 1(b)]. Surface tension γ and the complex shear modulus $G^*(\omega) = G'(\omega) + iG''(\omega)$ that characterize the droplet material properties can be obtained using a theoretical analysis of force balances associated with droplet deformation in the optical trap setup. Here G' and G'' denote the storage and loss moduli, respectively.

Force balance of droplet deformation.—The microrheology setup based on a dual optical trap is shown in Figs. 1(a), 1(b). The droplet is deformed by moving one trap. The resulting force balance involves forces F_1 and F_2 exerted on the droplet by the traps with stiffnesses k_1 and k_2, as well as viscous drag exerted on the droplet by the fluid with friction coefficient ξ [Fig. 1(c)]. In the overdamped regime, force balance requires
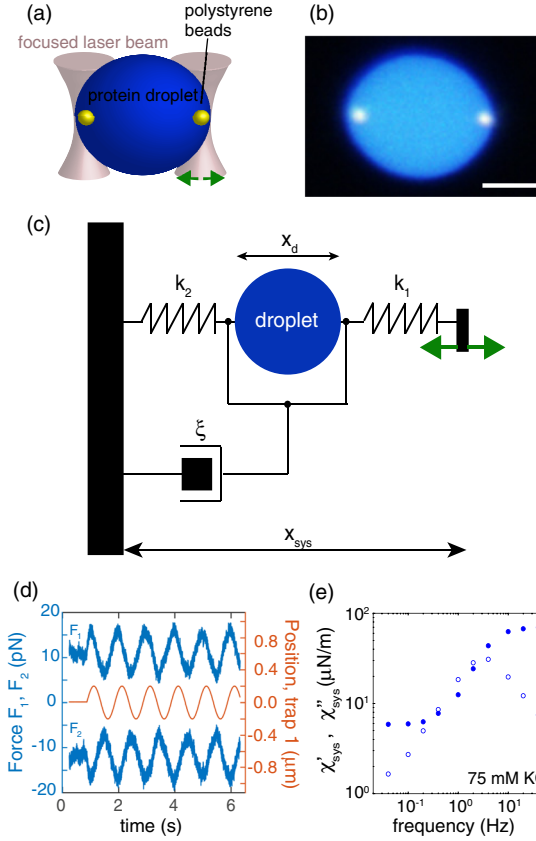
FIG. 1. Microrheology setup based on a dual optical trap. (a) Schematic. (b) Fluorescent micrograph of protein droplet during the measurement. Scale bar, 5 μm. (c) Mechanical circuit equivalent of measurement setup. (d) Exemplary experimental output during oscillatory droplet deformation: position of optical trap 1 (red) and forces associated to optical traps 1 and 2 (blue) at frequency 1 Hz and 75 mM KCl. (e) Exemplary system spring constants χ'_{sys} (filled circles), χ''_{sys} (empty circles) from the measurement of a protein droplet with a diameter of 12.2 μm at a salt concentration of 75 mM KCl.

$$F_1 + F_2 = \xi v, \qquad (1)$$

where v is the droplet velocity. The difference of F_1 and F_2 is balanced by forces exerted by the deformed droplet. For time periodic forces $F_{1,2} = \tilde{F}_{1,2} \exp(i\omega t) + \text{c.c.}$ and droplet diameter $x_d = x_{d,0} + \tilde{x}_d \exp(i\omega t) + \text{c.c.}$ with angular frequency ω, we have

$$(\tilde{F}_1 - \tilde{F}_2)/2 = \chi^*(\omega)\tilde{x}_d. \qquad (2)$$

Here, the tilde denotes the complex amplitude of the Fourier mode at angular frequency ω and c.c. refers to the complex conjugate. In Eq. (2), $\chi^*(\omega) = \chi'(\omega) + i\chi''(\omega)$ characterizes the complex frequency-dependent spring constant of the droplet response, where $\chi'(\omega)$ and $\chi''(\omega)$ denote the real and imaginary part of the complex spring constant, respectively. For an oscillatory trap movement $\tilde{v} = i\omega(\tilde{x}_d/2 + \tilde{F}_2/k_2)$. The complex spring constant of the entire system (droplet in series with two optical traps) is

$$\chi^*_{\text{sys}}(\omega) = (\tilde{F}_1 - \tilde{F}_2)/(2\tilde{x}_{\text{sys}}), \qquad (3)$$

where x_{sys} is the distance between the trap centers [Fig. 1(c)]. The distance x_{sys} can differ from the droplet diameter x_d because the beads can move out of the trap centers. The complex spring constant of the droplet can be related to the complex spring constant of the system using

$$x_{\text{sys}} = (F_1/k_1 - F_2/k_2) + x_d. \qquad (4)$$

We find

$$\chi^* = \frac{\chi^*_{\text{sys}}[4k_1k_2 + i\xi\omega(k_1 + k_2)]}{2k_1(2k_2 + i\xi\omega) - 4\chi^*_{\text{sys}}(k_1 + k_2 + i\xi\omega)}. \qquad (5)$$

Droplet mechanics in the optical trap.—To determine the protein droplet's surface tension γ as well as the complex frequency dependent shear modulus $G^*(\omega)$ in the optical trap setup, we need to relate these material properties to the complex spring constant χ^* defined in Eq. (2). The mechanical droplet stress satisfies the force balance

$$\partial_i \sigma_{ij} = 0. \qquad (6)$$

For small deformations in the low Reynold's number regime, the constitutive material equation of an incompressible droplet material can be written as

$$\tilde{\sigma}_{ij} = -\tilde{p} \cdot \delta_{ij} + G^*(\omega)[\partial_i \tilde{u}_j + \partial_j \tilde{u}_i], \qquad (7)$$

where p denotes pressure and u_i is the displacement vector with components $i, j = x, y, z$. Stress boundary conditions on the surface of a spherical droplet of radius R read in spherical coordinates r, θ, ϕ,

$$-p_{\text{ext}} - \sigma_{rr}(R, \theta) = 2\gamma H, \qquad (8)$$

$$\sigma_{r,\theta}(R, \theta) = 0. \qquad (9)$$

Here, p_{ext} is the local normal force per area exerted on the droplet surface and H denotes the mean curvature of the weakly deformed droplet surface. Forces mediated by adherent beads of radius r_{bead} are captured by a time periodic pressure distribution with complex amplitude $\tilde{p}_{\text{ext}} = P_0[\Theta(\theta - \pi + \theta_0) + \Theta(\theta_0 - \theta)]$ on the droplet surface [Fig. 2(a)], where Θ denotes the Heaviside function and $\theta_0 = r_{\text{bead}}/R$.

Using Eqs. (6)–(9), we calculate the time-dependent deformation field $u_r(r, \theta, t)$ of droplet material using a stream function approach and an expansion in spherical harmonics, see Supplemental Material [15]. The time dependent droplet diameter can be expressed as $x_d(t) = 2[R + u_r(R, 0, t)]$ and the difference of optical trap forces is given by $F_1(t) - F_2(t) = \oint dA\, p_{\text{ext}}$. We then obtain the
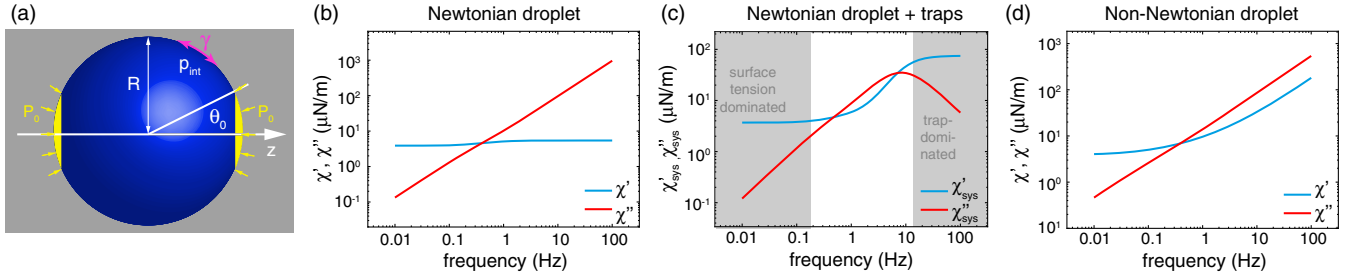
FIG. 2. Spring constants for a Newtonian and non-Newtonian droplet subject to polar forcing. (a) Droplets are subject to an oscillatory pressure P_0 applied in a dome-shaped region at the poles. (b) Complex spring constant χ^* of a Newtonian droplet with surface tension. (c) Complex system spring constant of a Newtonian droplet in series with two identical traps. For low frequencies, the spring constant is dominated by surface tension (gray zone, left-hand side). For high frequencies, the two traps dominate the spring constant and χ'_{sys} approaches $k/2$ (gray zone, right-hand side). Outside of this trap-dominated regime, the loss modulus is governed by the viscous properties of the droplet material. (d) Spring constant of a non-Newtonian droplet formed by a power law fluid, i.e., $G^*(\omega) = A\pi\omega^\beta[\csc(\pi\beta/2) + i\sec(\pi\beta/2)]/2$, and with surface tension. Parameters are $\theta_0 = 0.1$, $R = 5\ \mu m$, $\gamma = 3\ \mu N/m$, $\eta = 0.5\ Pa\,s$, $A = 0.2\ Pa$, $\beta = 0.8$, $k_1 = k_2 = 150\ pN/\mu m$, and $\xi = 6\pi\eta_b R$, where $\eta_b = 10^{-3}\ Pa\,s$.

complex spring constant of the droplet response χ^* as a function of G^* and γ using Eq. (2), see Supplemental Material [15]. This droplet spring constant is related to the spring constant of the entire optical trap system through Eq. (5).

Droplet spring constant in simple cases.—We first discuss the droplet and system spring constants for a droplet consisting of a Newtonian fluid. In this case, the complex shear modulus $G^* = i\omega\eta$, where η is the viscosity. Using the approach described above, we determine the droplet spring constant χ^* and the system spring constant χ^*_{sys}. The droplet spring constant as a function of frequency is shown in Fig. 2(b). The real part of the spring constant (blue) stems from surface tension. The imaginary part (red) is associated with viscosity.

The system spring constant for a Newtoninan droplet is shown in Fig. 2(c). At low frequencies, the response of the system is dominated by the droplet surface tension, corresponding to a plateau in the real part [see gray low-frequency region Fig. 2(c)]. The intermediate frequency range is dominated by droplet viscosity. At high frequencies, the system response is dominated by the optical traps [see gray high-frequency region Fig. 2(c)].

We also consider a droplet composed of a non-Newtonian fluid with a power law rheology in both loss and storage moduli $G' \sim G'' \sim \omega^\beta$ with exponent β. The corresponding droplet spring constant reveals droplet surface tension at low frequencies and power-law rheology at high frequencies, Fig. 2(d).

Salt dependent material properties of PGL-3 droplets.—We performed measurements on PGL-3 protein droplets formed in buffer (25 mM HEPES [4-(2-hydroxyethyl)-1-piperazineethanesulfonic acid], 1 mM DTT (dithiothreitol), pH 7.5) at four different salt concentrations (75, 115, 150, and 180 mM KCl). Polystyrene beads of 1 μm diameter added to the buffer were brought into adhesive contact with protein droplets (see Supplemental Material [15]). Radii of droplets used were between 5–9 μm.

Droplets were deformed at frequencies between 0.04 and 40 Hz. Forces exerted by both optical traps and the position of the mobile trap center were recorded. From this data, we first determined the system spring constant $\chi^*_{sys}(\omega)$ using Eq. (3) [Fig. 1(e)]. The frequency dependent spring constant exhibits the three regimes discussed above [compare Figs. 1(e) and 2(c)]: a low frequency regime dominated by surface tension, an intermediate regime and a high frequency regime dominated by the traps [Fig. 1(e)].

We then determined the complex spring constant of uniaxial droplet elongation χ^* using Eq. (5) [Fig. 3(a)]. From this data, we first determined the surface tension γ in the low frequency regime using

$$\gamma \approx \chi'(\omega)/(1.25 + 4.36\theta_0^2), \qquad (10)$$

valid for small $\theta_0 = r_{bead}/R \ll 1$ (see Supplemental Material [15]). We then obtain the complex shear modulus G^* by accounting for surface tension effects from the droplet spring constant [Fig. 3(b) and Supplemental Material [15]]. For modulus $R|G^*(\omega)| \gg \gamma$ and small θ_0 we use

$$G^*(\omega) \approx \frac{[\chi^*(\omega) - (1.75 + 6.31\theta_0^2)\gamma]}{R(0.58 + 3.42\theta_0^2)} \qquad (11)$$

(see Supplemental Material [15]). Figures 3(c)–3(f) show storage and loss moduli as a function of frequency averaged over several experiments for four different salt concentrations. Loss moduli G'' increased approximately linearly for increasing frequency [Figs. 3(b)–3(f)]. Corresponding viscosity values range from $\eta = 0.1$ to 1 Pa s. Storage moduli at a reference frequency of 10 Hz ranged between values of 0.1 and 15 Pa. Both viscosities and storage moduli decreased with increasing salt concentration [Figs. 3(g) and 3(i)]. The associated loss tangent G''/G' exhibited a sharp drop when salt concentration was reduced to 75 mM, suggesting a more solidlike rheology at lower salt concentrations [Fig. 3(j)].
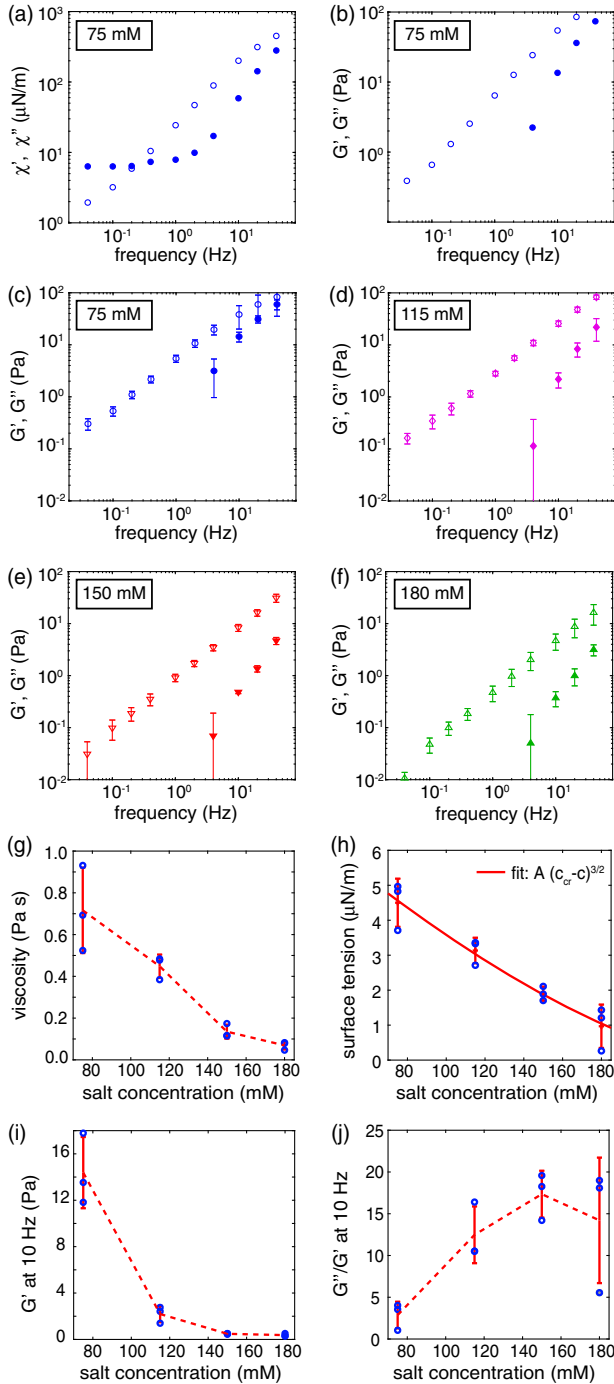
FIG. 3. Salt-dependent material properties of PGL-3 droplets. (a)–(b) Spring constants χ' (filled circles), χ'' (empty circles), and reconstructed moduli G' (filled circles), G'' (empty circles) for one droplet. [Corresponding χ^*_{sys} shown in Fig. 1(e)] (c)–(f) Ensemble average of G' (closed symbols), G'' (open symbols) of the droplet material at salt concentrations of 75, 115, 150, and 180 mM KCl. Error bars indicate standard deviations ($n = 3$). (g)–(j) Salt dependence of viscosity found using a linear fit to the loss modulus ($G'' = \omega\eta$, where η is the viscosity) (g), surface tension (h), storage modulus at 10 Hz (i), and loss tangent at 10 Hz (j). In panel (h), we show a fit of the theoretically predicted decay of surface tension in dependence of salt concentration c (solid red line) [26], where $c_{cr} = 243$ mM is the fitted critical salt concentration.

The estimated surface tension γ was about 5 μN/m for 75 mM salt and decreased steadily for increasing salt concentrations with $\gamma \approx 1$ μN/m at 180 mM salt [Fig. 3(h) and Supplemental Material [15]]. To test our new method, we measured viscosity and surface tension using two established methods. Using passive bead-tracking micorheology, we estimated a viscosity $\eta = 0.7 \pm 0.1$ Pa s at 75 mM salt, which is in excellent agreement with our active microrheology results [Fig. 3(g) and Supplemental Material [15]]. Furthermore, we analyzed thermal fluctuations of droplet shape to measure surface tension $\gamma \approx 1.4$ μN/m at 180 mM salt, consistent with our new method.

The surface tension and viscosity of polyelectrolyte condensates have been studied theoretically [25,26]. In Fig. 3(h), we compare the predicted salt dependence of surface tension to our data and find good agreement. Furthermore, the salt dependence of a characteristic time is also in agreement with this theory (see Fig. S6 in the Supplemental Material [15]).

Discussion.—Here, we used a novel technique with optical traps to characterize the rheology of PGL-3 protein droplets. We find that newly formed PGL-3 droplets consist of a viscoelastic material with liquidlike material properties that depend on salt concentration. Viscosities range from 0.1 to 1Pa s for decreasing salt concentrations from 180 to 75 mM. The storage modulus is smaller than the loss modulus, but approaches the loss modulus from below for frequencies larger than 10 Hz. Furthermore, we obtain more precise values of surface tension than previous methods. Values depend on salt concentration and range from 1 to 5 μN/m for decreasing salt concentrations from 180 to 75 mM. Such low values of surface tension are consistent with values estimated for colloidal systems with weak interactions but much smaller than typical air-water or oil-water systems [27]. Notably, our viscosity and surface tension estimates for PGL-3 droplets *in vitro* are consistent with estimates for P granules *in vivo* suggesting that *in vitro* PGL-3 is a good model system for the physics and material properties of P granules *in vivo* [2]. Interestingly, our viscosity and surface tension values for PGL-3 are between 1 and 2 orders of magnitude smaller than estimates for droplets of the P-granule protein LAF-1 formed *in vitro* [12].

Viscosities of PGL-3 droplets exhibit a strong salt dependence qualitatively similar to salt-dependent viscosity estimates reported for phase-separated LAF-1 by passive bead-tracking microrheology [Fig. 3(g)] [12]. The decrease in storage moduli, loss moduli, and surface tensions for increasing salt concentrations suggests that screened electrostatic interactions play an important role in protein condensates and their material properties. As salt concentration is increased, interactions become weaker because of screening effects. Interestingly, synthetic polyelectrolytes show a similar dependence of rheology and surface tension on salt concentration as the protein condensates studied here [25,26].

In conclusion, our measurements show that protein condensates are complex polymeric liquids with viscoelastic material properties that can be regulated by salt concentration. We obtain our results using a novel optical trap based rheometer suitable for micron-sized probes. This method does not rely on thermodynamic equilibrium. We expect that our work will trigger more studies that lead to a deep understanding of the physics of protein droplets and their phase behavior in biological cells.

[*]Corresponding author.
julicher@pks.mpg.de
[†]Corresponding author.
elisabeth.fischer-friedrich@tu-dresden.de

[1] A. A. Hyman, C. A. Weber, and F. Jülicher, Annu. Rev. Cell Dev. Biol. **30**, 39 (2014).

[2] C. P. Brangwynne, C. R. Eckmann, D. S. Courson, A. Rybarska, C. Hoege, J. Gharakhani, F. Jicher, and A. A. Hyman, Science **324**, 1729 (2009).

[3] C. P. Brangwynne, T. J. Mitchison, and A. A. Hyman, Proc. Natl. Acad. Sci. U.S.A. **108**, 4334 (2011).

[4] N. Gilks, N. Kedersha, M. Ayodele, L. Shen, G. Stoecklin, L. M. Dember, and P. Anderson, Mol. Biol. Cell **15**, 5383 (2004).

[5] A. Patel, H. O. Lee, L. Jawerth, S. Maharana, M. Jahnel, M. Y. Hein, S. Stoynov, J. Mahamid, S. Saha, T. M. Franzmann, A. Pozniakovski, I. Poser, N. Maghelli, L. A. Royer, M. Weigert, E. W. Myers, S. Grill, D. Drechsel, A. A. Hyman, and S. Alberti, Cell **162**, 1066 (2015).

[6] S. Saha, C. A. Weber, M. Nousch, O. Adame-Arana, C. Hoege, M. Y. Hein, E. Osborne-Nishimura, J. Mahamid, M. Jahnel, L. Jawerth, A. Pozniakovski, C. R. Eckmann, F. Jicher, and A. A. Hyman, Cell **166**, 1572 (2016).

[7] Y. Lin, D. S. W. Protter, M. K. Rosen, and R. Parker, Mol. Cell **60**, 208 (2015).

[8] S. F. Banani, A. M. Rice, W. B. Peeples, Y. Lin, S. Jain, R. Parker, and M. K. Rosen, Cell **166**, 651 (2016).

[9] T. Murakami et al., Neuron **88**, 678 (2015).

[10] T. Nott, E. Petsalaki, P. Farber, D. Jervis, E. Fussner, A. Plochowietz, T. D. Craggs, D. Bazett-Jones, T. Pawson, J. Forman-Kay, and A. Baldwin, Mol. Cell **57**, 936 (2015).

[11] S. T. Aoki, A. M. Kershner, C. A. Bingman, M. Wickens, and J. Kimble, Proc. Natl. Acad. Sci. U.S.A. **113**, 1279 (2016).

[12] S. Elbaum-Garfinkle, Y. Kim, K. Szczepaniak, C. C. -H. Chen, C. R. Eckmann, S. Myong, and C. P. Brangwynne, Proc. Natl. Acad. Sci. U.S.A. **112**, 7189 (2015).

[13] A. Molliex, J. Temirov, J. Lee, M. Coughlin, A. P. Kanagaraj, H. J. Kim, T. Mittag, and J. P. Taylor, Cell **163**, 123 (2015).

[14] C. P. Brangwynne, P. Tompa, and R. V. Pappu, Nat. Phys. **11**, 899 (2015).

[15] See Supplemental Material at http://link.aps.org/supplemental/10.1103/PhysRevLett.121.258101 for movies, materials, methods, and mathematical derivations, which includes Refs. [16–24].

[16] P. H. Jones, O. M. Marag, and G. Volpe, *Optical Tweezers: Principles and Applications* (Cambridge University Press, Cambridge, England, 2015).

[17] A. Farré, F. Marsà, and M. Montes-Usategui, Opt. Express **20**, 12270 (2012).

[18] J. Schindelin, I. Arganda-Carreras, E. Frise, V. Kaynig, M. Longair, T. Pietzsch, S. Preibisch, C. Rueden, S. Saalfeld, and B. Schmid, Nat. Methods **9**, 676 (2012).

[19] S. Ljunggren and J. Christer Eriksson, J. Chem. Soc., Faraday Trans. 2 **80**, 489 (1984).

[20] T. Betz and C. Sykes, Soft Matter **8**, 5317 (2012).

[21] D. J. Acheson, *Elementary Fluid Dynamics* (Clarendon Press, Oxford, 1990).

[22] A. Mietke, O. Otto, S. Girardo, P. Rosendahl, A. Taubenberger, S. Golfier, E. Ulbricht, S. Aland, J. Guck, and E. Fischer-Friedrich, Biophys. J. **109**, 2023 (2015).

[23] L. D. Landau and E. M. Lifshitz, *Fluid Mechanics*, 2nd ed. (Pergamon Press, Kronberg, 1987).

[24] L. Haberman and R. Sayre, *Model Basin Rep.* edited by D. Taylor (1958).

[25] E. Spruijt, J. Sprakel, M. Lemmers, M. A. C. Stuart, and J. van der Gucht, Phys. Rev. Lett. **105**, 208301 (2010).

[26] E. Spruijt, J. Sprakel, M. A. C. Stuart, and J. v. d. Gucht, Soft Matter **6**, 172 (2010).

[27] D. G. A. L. Aarts, M. Schmidt, and H. N. W. Lekkerkerker, Science **304**, 847 (2004).